

Highlights

Rethinking the Need for Source Models: Source-Free Domain Adaptation from Scratch Guided by a Vision-Language Model

Zhou Bingtao, Xiang Mian, Ning Qian*

- **Research highlight 1** We introduce ViL-Only Domain Adaptation (VODA), a strictly source-information-free paradigm that eliminates reliance on both source data and source models. VODA operates solely with a randomly initialized model, a vision-language model, and unlabeled target data. Through geometric analysis of the adaptation dynamics, we uncover a convergent behavior: under strong vision-language guidance, models initialized from vastly different states converge to nearly identical final representations. This finding questions the foundational necessity of source model initialization in current SFDA and opens a new, more accessible direction for domain adaptation.
- **Research highlight 2** We propose Two-Stage Denoised-Region Distillation (TS-DRD), a novel framework that first warms up the model using pure vision-language guidance, then constructs a theoretically-grounded Denoised-Region to suppress noise and produce cleaner supervision for distillation. TS-DRD achieves state-of-the-art or highly competitive performance across Office-Home, VisDA, and DomainNet-126, outperforming even source-dependent SFDA methods, while introducing negligible computational overhead.

Rethinking the Need for Source Models: Source-Free Domain Adaptation from Scratch Guided by a Vision-Language Model

Zhou Bingtao^{a,b}, Xiang Mian^b, Ning Qian^{*a}

^a*Sichuan University, No.24 South Section 1, Yihuan Road, Chengdu, 610065, Sichuan, China*

^b*Hubei Minzu University, 39 Xueyuan Road, Enshi, 445000, Hubei, China*

Abstract

Source-Free Domain Adaptation (SFDA) adapts source models to target domains without accessing source data, addressing privacy and transmission issues. However, existing methods still initialize from a source pre-trained model and thus are not truly source-free. Recent works have introduced Vision-Language (ViL) models to guide the adaptation process, in these methods, we observe that for the same target domain, different source models yield minimal variation in final results, indicating the source model itself has limited impact. Motivated by this, we propose ViL-Only Domain Adaptation (VODA), a stricter setting that **eliminates all dependencies on source domain**, relying solely on a randomly initialized model, a ViL model, and unlabeled target data. We analyze the adaptation dynamics of VODA and introduce Two-Stage Denoised-Region Distillation (TS-DRD), a two-stage framework that first warms up the model with ViL guidance, then seek a Denoised-Region inherent in both the ViL and adapting model, yielding cleaner supervision for distillation. Experiments on Office-Home, VisDA, and DomainNet-126 show that under VODA, TS-DRD achieves competitive or superior performance to existing SFDA methods that still use source models, demonstrating its effectiveness and the potential of the VODA setting.

Keywords: domain adaptation, Vision-Language-Model, source-free domain adaptation

1. Introduction

Source-Free Domain Adaptation (SFDA) tackles the challenge of adapting a model to an unlabeled target domain without access to source data, which is often required in privacy-sensitive scenarios [1, 2, 3]. Despite being termed "source-free", this paradigm is not entirely free of source information, as the source data and labels are required to train the source model in the first place, and the source domain's characteristics are implicitly embedded within the model's parameters.

Recent works leverage Vision-Language (ViL) models as an external guide for the adaptation process [4, 5, 6]. By providing high-quality supervision signals from ViL models, these methods significantly improve the adaptation performance. However, we observe a thought-provoking phenomenon in this line of work: when a powerful ViL model is employed for guidance, the final adaptation performance on the same target domain shows a surprisingly weak dependence on different source models. For instance, as shown in Figure 1a of the current state-of-the-art approach method ProDe [5], the results of adapting from different source domains to the same target domain exhibit minimal variance, with statistically insubstantial differences. Other work like DIFO [4] and DTKI [6] also shows very small differences across different source domains on the same target domain adaptation task, and across multiple datasets, differences exceeding 2% are rare. This indicates that in ViL model' guided SFDA methods, the domain-specific information carried by the source model plays a negligible role in determining the final outcome.

This observation encourages us to rethink the necessity of this prevailing SFDA paradigm: If the impact of the source models is so marginal, is it possible to discard them altogether to achieve a truly source-free adaptation? To this end, we propose a new learning setting: training the target model from scratch using only an untrained initial model, a ViL model and unlabeled target data, termed ViL-Only Domain Adaptation (VODA), as illustrated in Figure 1b. In this setting, dependencies of information and resources on source domain is thoroughly eliminated, thus achieving genuine source-information-free adaptation.

In this paper, we first propose a dynamic process for VODA, which captures a key

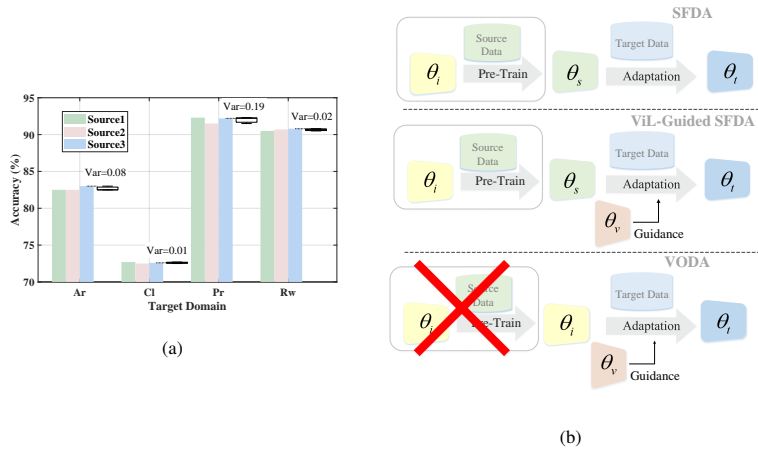


Figure 1: (a) Performance of ViL-guided SFDA methods (e.g., ProDe [5] in Office-Home) exhibits minimal variance across different source domains for the same target domain, indicating weak dependence on the source model. (b) Our proposed VODA setting: a truly source-free adaptation paradigm that eliminates all source dependencies.

insight: under proper ViL model’s guidance, the initial domain’s position becomes less critical to the final adaptation objective. This claim is empirically validated in our experiments. Guided by this dynamic perspective, the central challenge of VODA becomes how to leverage ViL model’s guidance at different stages of the adaptation trajectory. So we propose TS-DRD, a two-stage framework. It first uses pure ViL guidance to warm up the adapting model, then in the second stage, we construct a Denoised-Region by exploiting the complementary of both models, providing cleaner supervision for adaptation. Our contributions are summarized as follows:

- We propose ViL-Only Domain Adaptation (VODA), a novel and stricter adaptation setting that eliminates any dependency on source domains, and characterize its adaptation dynamics.
- Inspired by the dynamic process analysis of VODA, we propose TS-DRD, a two-stage framework that progressively transfers knowledge from the ViL model to the target model for stable and efficient adaptation.
- Experiments on Office-Home, VisDA, and DomainNet-126 show that TS-DRD performs on par with or outperforms state-of-the-art SFDA approaches, all with-

out leveraging any source information. This demonstrates the feasibility of VODA, establishing it as a viable paradigm for truly source-free adaptation. The code can be found in <https://github.com/Zhoubingtao/VODA-TS-DRD>.

2. Related Work

2.1. Traditional Source-Free Domain Adaptation

A dominant strategy of SFDA is self-training, which generates pseudo-labels on target data for supervision. Pioneering works like SHOT [1] established a baseline by aligning target features with the source hypothesis via information maximization. Following its idea, a major research thrust has focused on denoising these pseudo-labels using techniques such as neighborhood consistency [7], adaptive thresholding [8], or noise transition modeling [9]. Other approaches generate surrogate supervision through data synthesis [10, 11] or selective sampling [12, 13]. Crucially, the pseudo-labels generated in all these methods are fundamentally grounded in the knowledge encoded within the source-pretrained model. Consequently, they are "source-free" only in terms of data access but still rely on source models, making it inherently difficult to achieve genuine "source-information-free" adaptation.

2.2. ViL-Guided Source-Free Domain Adaptation

Large-scale ViL models like CLIP [14], with their strong zero-shot generalization, offer a powerful external prior for SFDA. A common strategy is to adapt the ViL model to the target domain via prompt tuning [15, 16, 17] and then leverage it to guide the adaptation of the source model. Recently, several methods have integrated ViL models into the SFDA pipeline. These works, such as DIFO [4] and ProDe [5], typically follow a hybrid paradigm: they use the adapted ViL model to provide high-quality supervised signals to adapt the source-pretrained model. Other methods, like DTKI [6], transfer CLIP's structural knowledge to the source model. However, our data analysis of these methods reveals a telling phenomenon: when adapting from different source domains to the same target domain, the final accuracy exhibits minimal variance. This reveals an essential source-model-irrelevant characteristic of this paradigm, implying

that its advantage stems primarily from its ViL model’s guidance. This key observation suggests a promising opportunity: to discard the source model entirely and realize a stricter, total source information free setting.

3. Method

3.1. Dynamic Process of VODA

This section develops a geometric dynamic process of VODA. We abstract the feature spaces occupied by different models as areas in a high-dimensional space. The definitions are as follows:

- Target Domain D_t : Represents the feature distribution of the target data.
- ViL Domain D_v : Represents the feature distribution of a pre-trained ViL model. Benefiting from its strong generalization learned from large-scale cross-modal data, we assume its distance to D_t , show as $d_{v \rightarrow t}$, is relatively small.
- Source Domain D_s : Represents the distribution of a pre-trained source model. Its distance to the target domain is $d_{s \rightarrow t}$.
- Initial Domain D_i : Represents a randomly initialized model. Its distance to the target domain, $d_{i \rightarrow t}$, is typically greater than $d_{s \rightarrow t}$.

As shown in Figure 2, the adaptation process from an initial point (D_s or D_i) to the target domain D_t can be decomposed into the vector sum of two key components:

- The ViL guidance component \vec{G}_v : It points towards the ViL domain D_v , representing the high-quality guidance provided by the ViL model.
- The direct target adaptation component \vec{G}_t : It represents the domain-specific information learned directly from target data. Due to substantial domain shift, \vec{G}_t may significantly deviate from the true target direction.

Therefore, the complete adaptation direction \vec{G} from any initial point D_x (where $x \in \{s, i\}$) can be expressed as:

$$\vec{G} = \vec{G}_v + \vec{G}_t \tag{1}$$

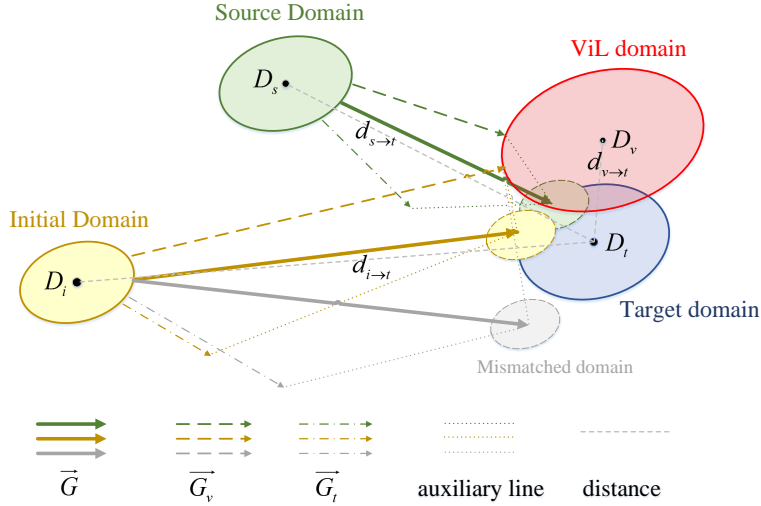


Figure 2: Illustration of the dynamic adaptation process: ViL guidance drives models from distinct initial domains toward a shared target representation.

Since both $d_{i \rightarrow t}$ and $d_{s \rightarrow t}$ are significantly larger than $d_{v \rightarrow t}$, the most informative supervision in the VODA setting is from \vec{G}_v . This implies that when \vec{G}_v is sufficiently strong, both D_i and D_s will gradually approach D_v , and thereby also move closer to D_t , which is illustrated by the model convergence depicted in Figure 2. Based on this, we formalize the following Hypothesis:

Hypothesis 1 In SFDA, given a powerful ViL model’s guidance, models starting from different initial points (e.g., D_s or D_i) will converge to similar states in their final predictive distributions.

We will provide detailed validation of **Hypothesis 1** in the subsection 4.7.

From **Hypothesis 1**, we obtain a fundamental guideline for VODA: the adaptation process should strengthen the \vec{G}_v guidance, and concurrently limit the contribution of \vec{G}_t when the model remains distant from D_t . This strategy ensures that the model does not converge to a mismatched domain, as depicted in Figure 2.

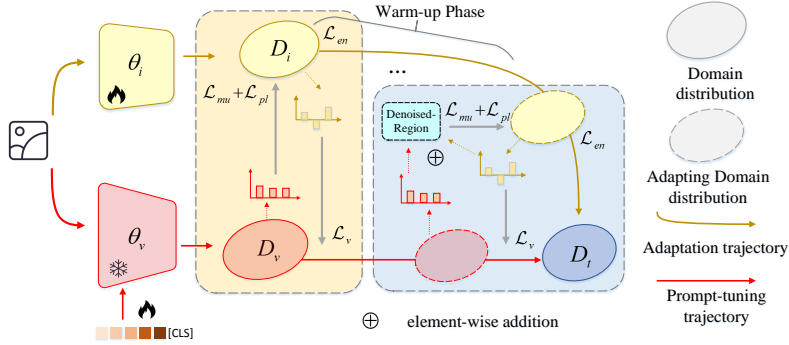


Figure 3: Overview of the TS-DRD framework. Stage 1 (Warm-up): the ViL model provides initial supervision to guide the target model toward the target domain. Stage 2 (Denoised-Region Transfer): The predictions of both the adapting model and the ViL model are jointly leveraged to generate a Denoised-Region, improving signal quality for subsequent distillation.

3.2. Problem Definition and Overview

Problem Definition We consider a scenario where we have unlabeled target data, containing C classes in total. Let $\mathcal{X}_t = \{x_i\}_{i=1}^T$ represent the unlabeled target samples, where T is the number of target samples. Instead of a source model θ_s in the SFDA setting, our adaptation process starts from θ_i , a random-weight model. Our objective is to adapt this initial model θ_i to the target domain using only \mathcal{X}_t and a ViL model θ_v for guidance.

Specifically, we employ CLIP [14] as our ViL model θ_v . Followed by [17], the output of the ViL model $\theta_v(x)$ reflects the cosine similarities between the image feature and the textual features of all candidate classes.

Overview Figure 3 illustrates the overall framework of our TS-DRD method, which is directly motivated by the dynamic adaptation process. TS-DRD is operationalized through two distinct stages, each addressing a key aspect of the VODA dynamics:

Stage 1: Warm-up Phase This stage corresponds to the early phase of the dynamic model where the initial point D_i is far from the target domain D_t . Since \vec{G}_t is noisy, we rely primarily on the strong semantic prior of the ViL model D_v to provide high-quality supervisory signals. This effectively realizes the dominant guidance component \vec{G}_v , accelerating the adapting model θ_i toward the target distribution.

Stage 2: Denoised-Region Transfer As the adapting model acquires task-specific awareness and moves closer to D_t , the task-misalignment noise inherent in the raw ViL model’ output is non-negligible. To mitigate this, we construct a Denoised-Region, which leverages the relative independence of noise patterns between the adapting model and the ViL model to produce cleaner supervision signals.

Concurrently, we adapt the ViL model’s prompts using the process from [17] to further tailor its guidance to the target task. In the following sections, we first present the theoretical insight of Denoised-Region, followed by a detailed description of TS-DRD.

3.3. Theoretical Insight of Denoised-Region

Although ViL model provides semantically rich guidance, its output $\theta_v(x)$ still contains noise due to a lack of task-specific alignment. As illustrated in the dynamic process of Figure 2, in the later stages of adaptation, although the $\theta_t(x)$ is primarily guided by \vec{G}_v , due to the presence of \vec{G}_t , its noise does not completely overlap with that of the $\theta_v(x)$, exhibiting a degree of independence. This observation motivates a strategy that leverages the complementary nature of the two signals to obtain more robust guidance.

For a sample x , the outputs for a given class c from $\theta_v(x)$ and the $\theta_t(x)$ can be formulated as:

$$o_v^c(x) = o^{c*}(x) + \epsilon_v^c, \quad o_t^c(x) = o^{c*}(x) + \epsilon_t^c \quad (2)$$

where $o^{c*}(x)$ is the underlying true signal, ϵ_v^c and ϵ_t^c are the noise from $\theta_v(x)$ and $\theta_t(x)$. Following the commonly used strategy in the fields of data fusion [18] and ensemble learning [19], we combine them via simple addition, the sum signal $o_{\text{sum}}^c(x)$ becomes:

$$o_{\text{sum}}^c(x) = o_v^c(x) + o_t^c(x) = 2o^{c*}(x) + (\epsilon_v^c + \epsilon_t^c) \quad (3)$$

The corresponding probability after the softmax function is:

$$q^c(x) = \text{softmax}(o_{\text{sum}}^c(x)) = \frac{e^{2o^{c*}(x)} \cdot e^{(\epsilon_v^c + \epsilon_t^c)}}{\sum_{j=1}^C e^{2o^{j*}(x)} \cdot e^{(\epsilon_v^j + \epsilon_t^j)}} \quad (4)$$

Where $\sum_{j=1}^C e^{2o^{j*}(x)} \cdot e^{(\epsilon_v^j + \epsilon_t^j)}$ is a constant, so the prediction of x is decided by $e^{2o^{c*}(x)} \cdot e^{(\epsilon_v^c + \epsilon_t^c)}$. We analyze two typical cases:

- **Aligned-Noise Case:** If ϵ_v^c and ϵ_i^c share the same sign for class c , both terms $e^{2\sigma^{**}(x)}$ and $e^{(\epsilon_v^c + \epsilon_i^c)}$ are amplified. Provided that ϵ_i^c is not excessively large, the aligned-noise case results in only limited impact on the final class-probability distribution.
- **Misaligned-Noise Case:** In such a case, ϵ_v^c and ϵ_i^c are unlikely to coincide, leading to a reduction in $(\epsilon_v^c + \epsilon_i^c)$, while $e^{2\sigma^{**}(x)}$ remains amplified. This creates a decisive shift in the probability toward the true signal, effectively filtering out the conflicting noises.

In summary, the Denoised-Region yields higher accuracy when the noise in $\theta_v(x)$ and $\theta_i(x)$ exhibits a degree of independence and remains within a reasonable magnitude. This aligns well with our two-stage design: the initial warm-up phase reduces the initially large noise in $\theta_i(x)$, preparing the model to construct Denoised-Region. We also give a validation of Denoised-Region theory in the subsection 4.7.

3.4. Two-Stage Denoised-Region Distillation (TS-DRD)

Building upon the above Dynamic Process and theoretical insight, we propose the TS-DRD framework.

Construction of Denoised-Region Given a target sample x_i , in the warm-up strategy (first N epochs), we use the predictions of the ViL model as Denoised region \mathbf{d}_i , and thereafter obtain the \mathbf{d}_i via the elemental addition of the output from θ_v and the initial model θ_i . It is formulated as:

$$\mathbf{d}_i = \begin{cases} \theta_v(x_i), & \text{if epoch} \leq N \\ \theta_v(x_i) \oplus \theta_i(x_i), & \text{if epoch} > N \end{cases} \quad (5)$$

where \oplus denotes element-wise addition. As analyzed in subsection 3.3, Denoised-Region amplifies the true signal while smoothing out the independent noise components, resulting in a more reliable pseudo-supervision signal.

Distillation via Denoised-Region We distill knowledge into the initial model θ_i

from the Denoised-Region \mathbf{d}_i using a composite loss.

$$\mathcal{L}_i = \overbrace{\alpha (-\mathbb{E}_{x_i \in \mathcal{X}_i} \mathbf{I}(\mathbf{q}_d, \mathbf{q}_i))}^{\mathcal{L}_{\text{mu}}} + \gamma \overbrace{\sum_{c=1}^C \bar{q}_c \log \bar{q}_c}^{\mathcal{L}_{\text{en}}} - \beta \overbrace{\mathbb{E}_{x_i \in \mathcal{X}_i} \sum_{c=1}^C \mathbb{1}[c = y_i] \log \mathbf{q}_{i,c}}^{\mathcal{L}_{\text{pl}}}. \quad (6)$$

where $\mathbf{q}_d = \text{softmax}(\mathbf{d}_i)$, $\mathbf{q}_i = \text{softmax}(\theta_i(x_i))$, $y_i = \arg \max_c \mathbf{q}_{d,c}$, and \bar{q}_c is the mean predicted probability for class c over a batch. The three terms respectively enforce: (i) distribution alignment between the adapted ViL and the target model \mathcal{L}_{mu} , in practice, we approximate $\mathbf{I}(\cdot, \cdot)$ by the mutual information [20] between the two distributions; (ii) class balanced predictions by \mathcal{L}_{en} , followed by [21]; and (iii) pseudo-label supervision using the Denoised-Region \mathcal{L}_{pl} .

Prompt-based Adaptation of ViL Model Following the prompt learning paradigm [4, 5], we optimize a set of learnable context vectors so that the ViL model gains task-specific knowledge. The adaptation objective is a mutual-information maximization:

$$\mathcal{L}_v = -\mathbb{E}_{x_i \in \mathcal{X}_i} \mathbf{I}(\mathbf{q}_v, \mathbf{q}_i) \quad (7)$$

where $\mathbf{q}_v = \text{softmax}(\theta_v(x_i))$, the mutual information loss \mathcal{L}_v encourages high agreement between the ViL model’s prediction and \mathbf{q}_i .

The complete algorithm is outlined in Algorithm algorithm 1. Through this cooperative denoising and distillation procedure, TS-DRD enables robust adaptation from scratch under the VODA setting.

Algorithm 1: Training Process of TS-DRD

Input: Initial model θ_i , ViL model θ_v , target domain \mathcal{X}_t , total epochs To , warm-up epochs N , iterations per epoch M .

Output: Optimized initial model $\hat{\theta}_i$, customized ViL model $\hat{\theta}_v$.

For epoch = 1 to To do:

For m=1 to M:

 Sample a batch \mathcal{X}_t^b from \mathcal{X}_t and compute output of θ_i and θ_v .

if epoch $\leq N$ **then**

$d_i \leftarrow \theta_v(\mathcal{X}_t^b)$ // Warm-up with ViL model only

else

$d_i \leftarrow \theta_v(\mathcal{X}_t^b) \oplus \theta_i(\mathcal{X}_t^b)$ // Construct Denoised-Region

 Update θ_v 's learnable prompts by minimizing \mathcal{L}_v

 Update θ_i by minimizing \mathcal{L}_i .

End for

End for

Return $\hat{\theta}_i = \theta_i, \hat{\theta}_v = \theta_v$.

4. Experiments

4.1. Datasets

We test our approach on three widely-used domain adaptation datasets covering diverse scales and contexts:

- **Office-Home** [22] contains around 15,000 images across 65 categories. It includes four domains with notably different stylistic representations: Artistic (Ar), Clipart (Cl), Product (Pr), and Real-World (Rw) images.
- **VisDA** dataset [23] consists of 152k synthetic source images and 55k real-world target images sampled from Microsoft COCO [24], covering 12 object categories.
- **DomainNet-126** [25] includes approximately 145,000 images from 126 classes across four domains: Clipart (C), Painting (P), Real (R), and Sketch (S), and has been curated to minimize label noise present in the original DomainNet.

4.2. Competitors

We benchmark our method against numerous state-of-the-art approaches in domain adaptation.

- **Traditional SFDA Methods** We compare with a wide range of established SFDA techniques that do not utilize ViL models. These include: SHOT [1], NRC [7], GKD [26], HCL [11], AaD [27], AdaCon [28], CoWA [29], ELR [30], PLUE [31], CPD [32], TPDS [33], UCon-SFDA [34], and CADTrans [35].
- **ViL-Guided Methods** We also evaluate against methods that incorporate CLIP. Specifically, we compare with DAPrompt [15], PADCLIP-R [36], ADCLIP-R [37], DAMP-R [38], and PDA-R [39] from the Unsupervised Domain Adaptation (UDA) category, and DIFO-V [4], ProDe-V [5], and DTKI [6] from the SFDA category.

4.3. Implementation Details

Comparison Protocol For a given target domain, we compute the average accuracy achieved by a competitor method across all its reported source-to-this-target adaptation tasks. Then we compare TS-DRD with this averaged performance. In our evaluation, we report the results under the widely adopted closed-set protocol in Office-Home, VisDA, and DomainNet-126. Furthermore, since the VODA uses no source information, it can be regarded as open-set [40], so we also provide comparisons under the open-set protocol in Office-Home.

Frameworks The initial model θ_i is a standard convolutional network, serving as the starting point for adaptation, we use ResNet-50 [41] for Office-Home, and ResNet-101 [41] for VisDA and DomainNet-126, keeping consistency with the competitors. We initialized the networks using a layer-wise strategy: fully connected layers with Xavier uniform initialization [42], convolutional layers with Kaiming normal initialization tailored for ReLU activations [41], and batch normalization layers with weights set to 1 and biases to 0 [43]. The ViL model θ_v is instantiated using CLIP [14]. We employ its frozen vision encoder (e.g., ViT-B/32 [44]) as the image encoder and its

Table 1: Closed-set SFDA results (%) on **Office-Home**. SIF (source information-free) indicates whether the method requires any source information. **Bold** and underlined indicate the best results and the second best results.

Method	SIF	Venue	Target: Ar				Target: Cl				Target: Pr				Target: Rw				Avg.
			Cl	Pr	Rw→Ar	Avg.	Ar	Pr	Rw→Cl	Avg.	Ar	Cl	Rw→Pr	Avg.	Ar	Cl	Pr→Rw	Avg.	
SHOT [1]	×	ICML20	68.0	67.9	74.2	70.0	56.7	54.5	58.6	56.6	77.9	78.0	84.5	80.1	80.6	79.4	82.3	80.8	71.9
NRC [7]	×	NeurIPS21	68.1	65.3	71.0	68.1	57.7	56.4	58.6	57.6	80.3	79.8	85.6	81.9	82.0	78.6	83.0	81.2	72.2
GKD [26]	×	IROS21	68.7	67.6	74.4	70.2	56.5	54.8	58.5	56.6	78.2	78.9	84.8	80.6	81.8	79.1	82.6	81.2	72.2
AaD [27]	×	NeurIPS22	68.9	67.2	72.1	69.4	59.3	57.4	58.5	58.4	79.3	79.8	85.4	81.5	82.1	79.5	83.1	81.6	72.7
CoWA [29]	×	ICML22	69.1	67.7	72.8	69.9	56.9	57.2	60.5	58.2	78.4	80.0	84.5	81.0	81.0	79.9	82.4	81.1	72.5
ELR [30]	×	ICLR23	69.2	66.3	73.4	69.6	58.4	58.0	59.8	58.7	78.7	79.5	85.1	81.1	81.5	79.3	82.6	81.1	72.6
CPD [32]	×	PR23	68.5	67.9	73.8	70.1	59.1	57.9	61.2	59.4	79.0	79.7	84.6	81.1	82.4	79.5	82.8	81.6	73.0
TPDS [33]	×	IJCV24	70.6	69.8	74.5	71.6	59.3	56.8	61.2	59.1	80.3	79.4	85.3	81.7	82.1	80.9	82.1	81.7	73.5
CADTrans [35]	×	TIP25	83.1	80.1	81.8	81.7	70.3	62.9	74.3	69.2	88.7	90.2	92.5	90.5	90.0	89.9	90.5	90.1	82.9
UCon-SFDA [34]	×	ICLR25	78.6	80.2	83.2	80.7	65.6	65.9	69.1	66.9	87.8	79.3	88.7	85.3	91.0	87.6	87.3	88.6	80.3
CLIP (zero-shot) [14]	✓	ICML21	–	–	–	75.2	–	–	–	60.2	–	–	84.2	–	–	–	85.5	76.3	
PADCLIP-R [36]	×	ICCV23	77.8	76.3	78.1	77.4	57.5	59.2	60.2	58.9	84.0	85.5	86.7	85.4	83.8	84.7	85.4	84.6	76.6
ADCLIP-R [37]	×	ICCVW23	76.1	76.7	76.8	76.5	55.4	56.1	56.1	55.9	85.2	85.8	85.5	85.5	85.6	86.2	85.4	85.7	75.9
PDA-R [39]	×	AAAI24	75.2	74.2	74.7	74.7	55.4	55.2	55.8	55.5	85.1	85.2	86.3	85.5	85.8	85.2	85.8	85.6	75.3
DAMP-R [38]	×	CVPR24	76.6	76.3	77.0	76.6	59.7	59.6	61.0	60.1	88.5	88.9	89.9	89.1	86.8	87.0	87.1	87.0	78.2
DAPrompt [15]	×	TNNLS25	74.4	74.5	75.2	74.7	54.1	54.6	54.7	54.5	84.3	83.7	83.8	83.9	84.8	85.0	84.8	84.9	74.5
DIFO-V [4]	×	CVPR24	82.5	80.9	83.4	82.3	70.6	70.1	70.5	70.4	90.6	90.6	91.2	90.8	88.8	88.8	88.9	88.8	83.1
ProDe-V [5]	×	ICLR25	82.5	82.5	83.0	82.7	72.7	72.5	72.6	<u>72.6</u>	92.3	91.5	92.2	<u>92.0</u>	90.5	90.7	90.8	90.7	84.5
DTKI [6]	×	IPM26	82.3	82.8	82.7	<u>82.6</u>	72.0	71.1	71.1	71.4	91.7	91.9	91.6	91.7	90.0	90.0	90.3	90.1	84.0
TS-DRD (Ours)	✓	–	–	–	–	81.6	–	–	–	72.7	–	–	92.3	–	–	–	<u>90.5</u>	<u>84.3</u>	

frozen text transformer [45] as the text encoder, follow the process of compared methods [4, 5, 6].

Hyper-parameter Configuration All experiments use a batch size of 64 and optimize both the initial model θ_i and the ViL model θ_v via SGD with momentum 0.9. The learnable prompts are initialized as "a photo of a [CLASS]". Hyper-parameters are set as follows. On Office-Home, we use $\alpha = 1.3$, $\gamma = 1.0$, $\beta = 0.4$; on VisDA-C, $\alpha = 1.0$, $\gamma = 0.1$, $\beta = 0.4$; on DomainNet-126, $\alpha = 1.3$, $\gamma = 0.01$, $\beta = 0.4$. The learning rate is 1×10^{-3} for θ_i and 1×10^{-4} for θ_v across all benchmarks, the warm-up epoch number N is set to 4 for all benchmarks. Our framework is implemented in PyTorch and executed on NVIDIA RTX GPUs. Each adaptation task is repeated three times with different random seeds, and we report the average accuracy as the final result.

Table 2: Open-set SFDA results (%) on **Office-Home**. SIF (source information-free) indicates whether the method requires any source information. **Bold** and underlined indicate the best results and the second best results.

Method	SIF	Venue	Target: Ar				Target: Cl				Target: Pr				Target: Rw				Avg.
			Cl	Pr	Rw→Ar	Avg.	Ar	Pr	Rw→Cl	Avg.	Ar	Cl	Rw→Pr	Avg.	Ar	Cl	Pr→Rw	Avg.	
SHOT [1]	×	ICML20	63.1	65.3	69.6	66.0	64.5	59.3	64.6	62.8	80.4	75.4	82.3	79.4	84.7	81.2	83.3	83.1	72.8
HCL [11]	×	NeurIPS21	64.5	64.8	78.1	69.1	64.0	59.8	69.3	64.4	78.6	73.1	81.5	77.7	82.4	80.1	75.3	79.3	72.6
CoWA [29]	×	ICML22	67.6	66.9	68.5	67.7	63.3	56.9	57.9	59.4	79.2	83.6	85.9	82.9	85.4	82.0	81.1	82.8	73.2
AaD [27]	×	NeurIPS22	66.0	69.1	71.8	69.0	63.7	62.5	62.3	62.8	77.3	72.6	78.6	76.2	80.4	77.6	79.8	79.3	71.8
CLIP (zero-shot) [14]	✓	ICML21	–	–	–	75.2	–	–	–	60.2	–	–	84.2	–	–	–	85.5	76.3	
DIFO-V [4]	×	CVPR24	68.2	67.2	71.9	69.1	64.5	62.1	65.3	64.0	86.2	79.3	84.4	83.3	87.9	86.1	88.3	87.4	75.9
ProDe-V [5]	×	ICLR25	81.3	81.1	83.0	81.8	75.9	74.3	75.7	75.3	85.6	86.8	86.1	<u>86.2</u>	87.9	87.2	86.3	87.1	<u>82.6</u>
DTKI [6]	×	IPM26	77.5	77.9	79.1	78.2	70.1	68.2	71.5	69.9	84.4	85.1	85.5	85.0	87.9	86.3	88.7	<u>87.6</u>	80.2
TS-DRD (Ours)	✓	–	–	–	–	<u>81.6</u>	–	–	–	<u>72.7</u>	–	–	92.3	–	–	–	90.5	84.3	

4.4. Main Results

Office-Home (close-set) The results of Office-Home in close-set in shown in Table 1, our TS-DRD achieves an average accuracy of 84.3%. This performance is comparable to the best ViL-guided SFDA method, ProDe-V (84.5%), and significantly surpasses a range of traditional SFDA methods. Notably, TS-DRD attains the best accuracy on the Clipart (72.7%) and Product (92.3%) targets. Critically, TS-DRD requires no source model, yet it performs on par with state-of-the-art SFDA methods that initialize from source models, fully demonstrating the feasibility of the VODA paradigm.

Office-Home (open-set) In the open-set protocol, which is specifically designed for real-world scenarios, the source domain consists of only 25 classes while the target domain contains all 65 classes. From Table 2, under this challenging setting, most existing SFDA methods, including those guided by ViL models, suffer from significant performance degradation. In contrast, VODA setting is inherently total-open, it requires no knowledge of the source label set and assumes no relationship between source and target categories, making it truly ready for real-world deployment. Under this protocol, TS-DRD achieves an average accuracy of 84.3%, outperforming the second-best method ProDe-V (82.6%) by nearly 2%, further demonstrating its robustness and practical value.

VisDA Table 3 shows the results of VisDA, which is a challenging synthetic-to-

Table 3: Results (%) of closed-set SFDA on **VisDA**. SIF (source information-free) indicates whether the method requires any source information. **Bold** and underlined indicate the best results and the second best results.

Method	SIF	Venue	plane	bicycl	bus	car	horse	knife	mcycl	person	plant	sktbrd	train	truck	Per-class
Source	×	–	62.3	20.1	51.7	67.2	73.5	5.9	84.8	21.5	65.3	44.6	81.7	11.3	48.7
SHOT [1]	×	ICML20	95.0	87.4	80.9	57.6	93.9	94.1	79.4	80.4	90.9	89.8	85.8	57.5	82.7
NRC [7]	×	NeurIPS21	96.8	91.3	82.4	62.4	96.2	95.9	86.1	90.7	94.8	94.1	90.4	59.7	85.9
GKD [26]	×	IROS21	95.3	87.6	81.7	58.1	93.9	94.0	80.0	80.0	91.2	91.0	86.9	56.1	83.0
AaD [27]	×	NeurIPS22	97.4	90.5	80.8	76.2	97.3	96.1	89.8	82.9	95.5	93.0	92.0	64.7	88.0
AdaCon [28]	×	CVPR22	97.0	84.7	84.0	77.3	96.7	93.8	91.9	84.8	94.3	93.1	94.1	49.7	86.8
CoWA [29]	×	ICML22	96.2	89.7	83.9	73.8	96.4	97.4	89.3	86.8	94.6	92.1	88.7	53.8	86.9
ELR [30]	×	ICLR23	97.1	89.7	82.7	62.0	96.2	97.0	87.6	81.2	93.7	94.1	90.2	58.6	85.8
PLUE [31]	×	CVPR23	94.4	91.7	89.0	70.5	96.6	94.9	92.2	<u>88.8</u>	92.9	95.3	91.4	61.6	88.3
CPD [32]	×	PR23	96.7	88.5	79.6	69.0	95.9	96.3	87.3	83.3	94.4	92.9	87.0	58.7	85.5
TPDS [33]	×	IJCV24	97.6	91.5	89.7	<u>83.4</u>	97.5	96.3	92.2	82.4	<u>96.0</u>	94.1	90.9	40.4	87.6
UCon-SFDA [34]	×	ICLR25	98.4	90.7	88.6	80.7	97.9	96.9	93.1	83.8	97.6	95.9	92.6	59.1	89.6
CLIP (zero-shot) [14]	✓	ICML21	98.3	86.4	90.4	68.2	97.9	84.2	91.4	76.1	74.3	92.7	93.9	69.2	82.9
PADCLIP-R [36]	×	ICCV23	96.7	88.8	87.0	82.8	97.1	93.0	91.3	83.0	95.5	91.8	91.5	63.0	88.5
ADCLIP-R [37]	×	ICCVW23	98.1	83.6	91.2	76.6	<u>98.1</u>	93.4	96.0	81.4	86.4	91.5	92.1	64.2	87.7
PDA-R [39]	×	AAAI24	97.2	82.3	89.4	76.0	97.4	87.5	<u>95.8</u>	79.6	87.2	89.0	93.3	62.1	86.4
DAMP-R [38]	×	CVPR24	97.3	91.6	89.1	76.4	97.5	94.0	92.3	84.5	91.2	88.1	91.2	67.0	88.4
DAPrompt-R [15]	×	TNNLS25	97.8	83.1	88.8	77.9	97.4	91.5	94.2	79.7	88.6	89.3	92.5	62.0	86.9
DIFO-V [4]	×	CVPR24	97.5	89.0	<u>90.8</u>	83.5	97.8	97.3	93.2	83.5	95.2	<u>96.8</u>	93.7	65.9	90.3
ProDe-V [5]	×	ICLR25	98.3	<u>92.4</u>	86.6	80.5	<u>98.1</u>	98.0	92.3	84.3	94.7	97.0	94.1	75.6	<u>91.0</u>
DTKI [6]	×	IPM26	97.7	87.7	87.5	82.7	97.3	<u>98.3</u>	93.3	85.1	95.3	96.3	<u>94.0</u>	73.9	90.8
TS-DRD	✓	–	98.4	92.5	87.1	82.8	98.5	98.5	92.7	84.0	95.8	95.8	<u>94.0</u>	<u>74.5</u>	91.2

real dataset designed for practical domain adaptation. TS-DRD achieves state-of-the-art performance with an average accuracy of 91.2%, outperforming existing methods on categories like plane (98.4%), bicycle (92.5%), horse (98.5%) and knife (98.5%). Moreover, VODA accomplishes this without relying on any source-domain resources, saving the computational overhead typically required for synthetic data generation.

DomainNet-126 On the more extensive and diverse DomainNet-126 benchmark (Table 4), TS-DRD surpasses all compared methods with an average accuracy of 85.1%, and obtains the best performance on three of the four target domains: Clipart (85.8%), Painting (83.4%), and Real (92.6%). These results demonstrate that VODA and TS-DRD remain effective and powerful on larger datasets with more categories.

We also show the results of using CLIP [14] alone (zero-shot) in each dataset, where TS-DRD consistently and substantially outperforms its guidance source, clearly demonstrating the effectiveness of our adaptation approach.

Table 4: Closed-set SFDA results (%) on **DomainNet-126**. SIF (source information-free) indicates whether the method requires any source information. **Bold** and underlined indicate the best results and the second best results.

Method	SIF	Venue	Target: C				Target: P				Target: R				Target: S				Avg.
			P	R	S→C	Avg.	C	R	S→P	Avg.	C	P	S→R	Avg.	C	P	R→S	Avg.	
SHOT [1]	×	ICML20	67.9	67.7	70.2	68.6	63.5	67.6	64.0	65.0	78.2	81.3	78.0	79.2	59.5	61.7	57.8	59.7	68.1
GKD [26]	×	IROS21	69.6	68.3	71.5	69.8	61.4	68.4	65.2	65.0	77.4	81.4	77.6	78.8	60.3	63.2	59.5	61.0	68.7
NRC [7]	×	NeurIPS21	62.9	64.7	69.4	65.7	62.6	69.4	65.8	65.9	77.1	81.3	78.7	79.0	58.3	60.7	58.7	59.2	67.5
AdaCon [28]	×	CVPR22	62.2	63.1	67.1	64.1	60.8	68.1	66.0	65.0	74.8	78.3	75.4	76.2	55.9	58.2	55.6	56.6	65.4
CoWA [29]	×	ICML22	66.2	69.0	69.0	68.1	64.6	67.2	65.8	65.9	80.6	79.8	79.9	80.1	60.6	60.8	60.0	60.5	68.6
PLUE [31]	×	CVPR23	61.6	61.6	67.5	63.6	59.8	65.9	64.3	63.3	74.0	78.5	76.0	76.2	56.0	57.9	53.8	55.9	64.7
TPDS [33]	×	IJCV24	65.6	66.4	68.6	66.9	62.9	67.0	64.3	64.7	77.1	79.0	75.3	77.1	59.8	61.5	58.2	59.8	67.1
CADTrans [35]	×	TIP25	68.0	64.1	73.5	68.5	75.4	74.5	76.3	75.4	89.2	89.3	88.9	89.1	66.5	63.1	58.4	62.7	73.9
CLIP (zero-shot) [14]	✓	ICML21	–	–	–	77.3	–	–	–	76.2	–	–	–	88.6	–	–	–	71.1	78.3
ADCLIP-R [37]	×	ICCVW23	73.2	73.6	72.3	73.0	71.7	73.0	74.2	73.0	88.1	86.9	89.3	88.1	66.0	65.2	68.4	66.5	75.2
DAMP-R [38]	×	CVPR24	74.2	74.4	74.9	74.5	76.7	75.7	76.1	76.2	88.5	88.7	88.2	88.5	71.7	70.8	70.5	71.0	77.5
DAPrompt [15]	×	TNNLS25	72.7	73.2	73.8	73.2	72.4	72.4	72.9	72.6	87.6	87.6	87.8	87.7	65.9	65.6	66.2	65.9	74.8
DIFO-V [4]	×	CVPR24	80.0	80.8	80.5	80.4	76.6	77.3	76.7	76.9	87.2	87.4	87.3	87.3	74.9	75.6	75.5	75.3	80.0
ProDe-V [5]	×	ICLR25	85.0	85.5	85.5	<u>85.3</u>	83.2	83.1	83.4	<u>83.2</u>	92.4	92.3	92.4	<u>92.4</u>	79.0	79.3	79.1	79.1	<u>85.0</u>
DTKI [6]	×	IPM26	82.4	80.7	82.3	81.8	77.5	78.7	78.9	78.4	88.9	88.0	88.3	88.4	76.1	76.9	74.6	75.9	81.1
TS-DRD (Ours)	✓	–	–	–	–	85.8	–	–	–	83.4	–	–	–	92.6	–	–	–	<u>78.3</u>	85.1

Evaluation and Comparison on VODA setting To verify the unique effectiveness of TS-DRD in the VODA paradigm, we conduct experiments on all three datasets by re-implementing two ViL-guided SFDA methods, DIFO-V and ProDe-V, in the VODA scenario. Specifically, we replace their source models with randomly initialized ones and keep all other components unchanged. The results are summarized in Table 5.

Table 5: Comparison with state-of-the-art ViL-guided SFDA methods under the VODA setting. For reference, **Bold** indicates the best results under each setting.

Setting	Method	Office-Home	VisDA	DomainNet-126	Avg.
VODA	DIFO-V [4]	75.2	89.2	63.0	75.8
	ProDe-V [5]	83.0	54.7	82.0	73.3
	TS-DRD (Ours)	84.3	91.2	85.1	86.9

From Table 5, both DIFO-V and ProDe-V exhibit clear performance degradation under VODA. DIFO-V drops sharply on DomainNet-126 (63.0%), while ProDe-V fails catastrophically on VisDA (54.7%), confirming that directly applying existing

SFDA methods without source models leads to unstable and substantial performance loss, necessitating VODA-specific designs. In contrast, TS-DRD consistently outperforms both methods across all datasets, achieving the highest average accuracy of 86.9%. This superiority is attributed to our dynamic adaptation process and two-stage Denoised-Region distillation.

In summary, across diverse datasets with varying scales and domain gaps, our experiments consistently show that VODA is highly feasible, and TS-DRD successfully adapts a generic source-irrelevant model to target domains.

4.5. Ablation Study

We conduct an ablation study on the effectiveness of each component in TS-DRD, with the results summarized in Table 6.

The pseudo-label loss \mathcal{L}_{pl} is critical, as its removal reduces accuracy to nearly 1%. This confirms that ViL model provides the most direct and effective supervisory signal for knowledge transfer, without which the initial model fails to learn any meaningful representations. Removing the mutual-information alignment loss \mathcal{L}_{mu} or the entropy-minimization loss \mathcal{L}_{en} also result in clear decreases, indicating that aligning the ViL model’s output with the distribution of the Denoised-Region and encouraging balanced predictions are both important for stable adaptation.

Table 6: Ablation study on the effectiveness of different components in TS-DRD(%).

Configuration	Office-Home	VisDA-C	Domainnet126	Avg.
w/o \mathcal{L}_{pl}	1.2 (-83.1)	0.6 (-90.6)	1.1 (-84.0)	1.0 (-85.9)
w/o \mathcal{L}_{mu}	82.9 (-1.4)	90.1 (-1.1)	84.5 (-0.6)	85.8 (-1.1)
w/o \mathcal{L}_{en}	83.2 (-1.1)	90.3 (-0.9)	84.7 (-0.4)	86.1 (-0.8)
w/o Denoised-Region	82.2 (-2.1)	90.3 (-0.9)	83.1 (-2.0)	85.2 (-1.7)
w/o prompt tuning	82.9 (-1.4)	90.4 (-0.8)	83.0 (-2.1)	85.4 (-1.5)
w/o warm-up epoch	83.1 (-1.2)	90.9 (-0.3)	83.0 (-2.1)	85.7 (-1.2)
using source models	84.5 (+0.2)	91.0 (-0.2)	85.4 (+0.3)	87.0 (+0.1)
Full	84.3 (-)	91.2 (-)	85.1 (-)	86.9 (-)

Removing Denoised-Region (using ViL model’ output as Denoised-Region) causes a 1.7% drop, validating our theory in subsection 3.3. Disabling prompt tuning reduces

accuracy consistently, confirming that the adapting model is able to supply task-specific knowledge to the ViL model’s text side. And removing the warm-up phase leads to a noticeable performance degradation. Without warm-up, the initial model’s heavy noise corrupts the Denoised-Region.

We also examine the influence of different starting models under our TS-DRD framework. As shown in Table 6, when replacing the initial model with source models (SFDA setting), the performance across benchmarks remains highly similar. This minimal gap provides a preliminary empirical confirmation of **Hypothesis 1**. A more detailed and systematic validation of this dynamic behavior is presented in subsection 4.7.

4.6. Hyperparameter Sensitivity Analysis

We analyze the sensitivity of our TS-DRD framework to key hyperparameters on the Office-Home dataset (\rightarrow Cl). Figure 4 presents 3D surface plots of the average accuracy as functions of (α, γ) and (β, N) .

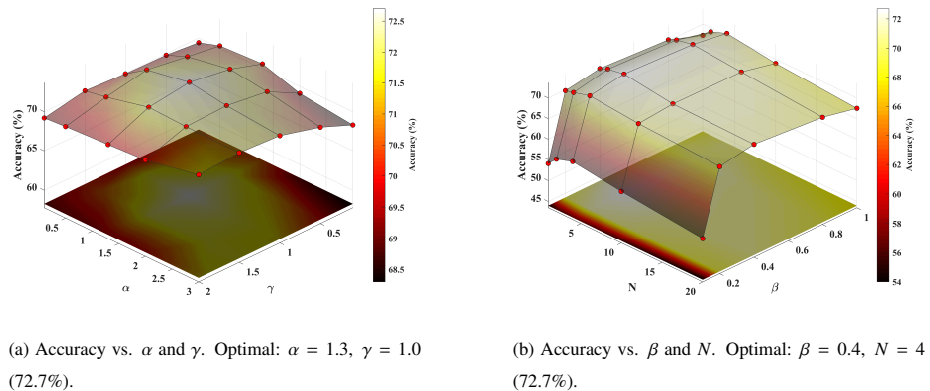


Figure 4: Hyperparameter sensitivity analysis on Office-Home. (a) Varying mutual information weight α and entropy weight γ . (b) Varying pseudo-label weight β and number of warm-up epochs N .

Analysis of α and γ . Parameters vary as $0.5 \leq \alpha \leq 3.0$ and $0.1 \leq \gamma \leq 2.0$ with step 0.1. As shown in Figure 4a, accuracy remains stable within a moderate range but degrades at the boundaries: Extreme values, such as $\alpha = 3.0$ or $\gamma = 2.0$, lead to degradation, which suggests that within a broad range, neither α nor γ provides direct

supervision signals and thus contribute little to the dominant guidance component \vec{G}_v .

Analysis of β and N . We analyze β and N with $\beta \in [0.1, 1.0]$ and $N \in [1, 20]$. As Figure 4b illustrated, the model is particularly sensitive to small β : when β drops to 0.2, the accuracy decreases dramatically. According to the dynamic process, the adapting model initially relies heavily on ViL guidance \vec{G}_v to approach the target. A small β weakens the Denoised-Region supervision, reducing the influence of \vec{G}_v and allowing the model to drift due to its own noise. For warm-up, insufficient $N < 4$ leaves high initial noise that corrupts the Denoised-Region; $N \geq 4$ stabilizes the performance (only a slight drop in $N = 20$), indicating that a moderate warm-up suffices and a further extension yields diminishing returns.

4.7. Experimental Verification of the Dynamic Process

To experimentally validate the dynamic process and theoretical analysis discussed above, we conduct adaptation on the Office-Home benchmark under the Pr→Cl task, VisDA and DomainNet-126 (P→C task), starting from a source model D_s , using our TS-DRD method under the SFDA setting. We systematically compare it with our result under VODA setting, illustrating the adaptation trajectories and final convergence behaviors.

Validation of Hypothesis 1 To fully verify **Hypothesis 1**, which presents the dynamic process of VODA, we present the following two group of figures:

Figure 5a displays the accuracy curves (left axis) and the Jensen–Shannon divergence (JSD) between the predictions of the source and initial models (right axis) on Office-Home. Both models converge to approximately 72% accuracy under the guidance of the ViL model, visually demonstrating that the final performance is insensitive to the starting point. The JSD drops from about 0.3 to nearly 0.05, entering the regime of high agreement (JSD < 0.1 typically indicates very similar distributions, while values above 0.3 indicate substantial divergence). This consistent reduction confirms, from a distribution-alignment perspective, that the two models become increasingly similar during adaptation. The same pattern holds on VisDA (Figure 5d) and DomainNet-126 (Figure 5g), where both models converge to comparable accuracy levels and the JSD decreases substantially, fully supporting **Hypothesis 1**.

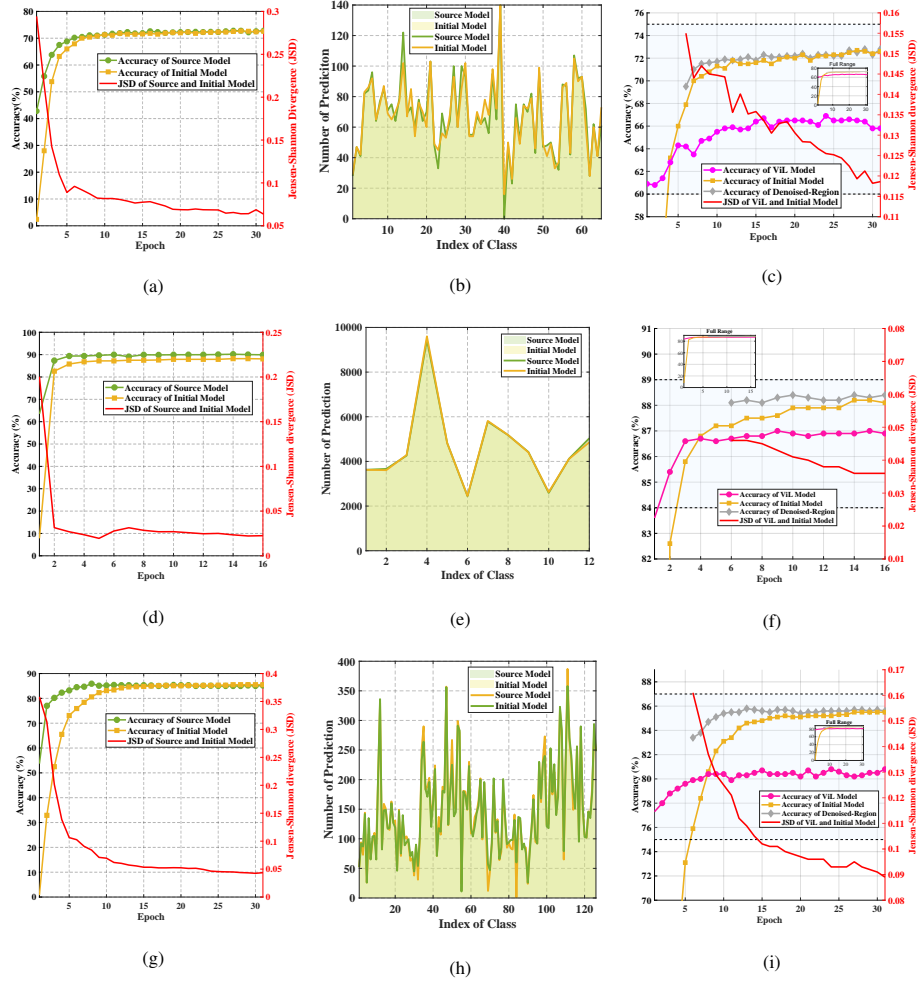


Figure 5: Validation on multiple domain adaptation benchmarks. (a, d, g): Accuracy (left axis) and JSD (right axis) of source and initial models on Office-Home (Pr→Cl), VisDA, and DomainNet-126 (P→C), validating their convergent predictions under ViL guidance. (b, e, h): Final per-class prediction counts, showing near-identical distributions. (c, f, i): Accuracy of the ViL model, adapting model, and Denoised-Region (left axis), with noise JSD between models (right axis), demonstrating the inverse relation between noise independence and Denoised-Region gain.

Figure 5b, Figure 5e, and Figure 5h present the per-class prediction counts at the final training epoch. Across Office-Home, VisDA, and DomainNet-126, the curves for the source and initial models overlap almost perfectly and the shaded regions between them are barely visible, providing strong visual evidence that the final predictions become virtually identical, again in agreement with **Hypothesis 1**.

Validation of Denoised-Region Theory To validate the Denoised-Region theory in subsection 3.3, Figure 5c plots the accuracy curves of θ_i , θ_v and Denoised-Region (left axis) on Office-Home. After the warm-up phase, the Denoised-Region consistently outperform both models, validating the effectiveness of it.

We also show the JSD between the noise distributions of θ_i and θ_v (right axis). Followed by Equation 2, the noises are formulated as: $\text{softmax}(|\theta_i(x)-y|)$, $\text{softmax}(|\theta_v(x)-y|)$, where y is the one-hot logits of the true label. The performance gain of Denoised-Region over individual models exhibits a clear inverse relationship with the JSD: larger gains are observed when JSD is higher, indicating stronger noise independence between the two models. As JSD decreases, the accuracy of Denoised-Region gradually converges to that of the better single model, consistent with our theoretical analysis.

The same pattern holds on VisDA (Figure 5f) and DomainNet-126 (Figure 5i). On VisDA, the Denoised-Region again surpasses the individual models, with the largest improvement observed when the noise JSD is high. Although the accuracy gap among models is relatively small on this dataset, the inverse relation between gain and noise JSD remains visible. On DomainNet-126, the gains are even more pronounced due to larger initial noise discrepancies, and the inverse correlation is clearly evident. These consistent results across benchmarks further validate our Denoised-Region theory.

4.8. Feature Visualization

We further visualize the feature distributions of the target domain after adaptation using t-SNE. Figure 6 compares four models on the Office-Home Cl→Ar task: a randomly initialized model, SHOT (a traditional SFDA method), ProDe-V (state-of-the-art ViL-guided SFDA), and our TS-DRD.

The initial model yields completely unstructured features. SHOT improves the separation, yet still produces relatively dispersed clusters. And both ProDe-V and our

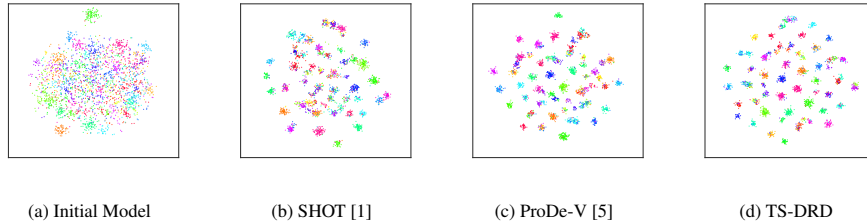


Figure 6: 2D t-SNE visualization of feature distributions on Cl→Ar task in Office-Home dataset: (a) Initial model; (b) SHOT; (c) ProDe-V; (d) TS-DRD.

TS-DRD generate compact, well-separated clusters, and their feature distributions are nearly indistinguishable. This observation at the feature-level validates the effectiveness of our method and confirms the feasibility of the VODA setting.

4.9. Training Resource Consumption Comparison

We compare the GPU memory consumption (peak GPU memory consumption during training) and training times (per iteration) of our TS-DRD with ProDe-V under the same experimental setting (batch size 64, on Office-Home Pr→Cl).

Table 7: GPU memory consumption and Training times on Office-Home Pr→Cl.

Method	GPU memory consumption (GB)	training time (s)
ProDe-V [5]	10.96	0.23
TS-DRD (Ours)	10.68	0.22

As reported in Table 7, the two methods exhibit nearly identical memory consumption. Moreover, TS-DRD achieves a faster training speed, requiring only 0.22 seconds per iteration compared to 0.23 seconds for ProDe-V. This demonstrates that our two-stage Denoised-Region distillation does not introduce additional computational overhead compared to existing ViL-guided SFDA approaches. The overall memory requirement remains moderate, confirming that VODA is resource-friendly, making it suitable for practical deployment.

5. Conclusion

This paper proposes VODA, a truly source-free setting that uses only an untrained initial model, a ViL model, and unlabeled target data, requiring no source information. Through a dynamic geometric model, we show that, under strong ViL guidance, the starting point has little effect on final performance. This insight motivates our two-stage TS-DRD design: a warm-up phase that establishes reliable supervision using pure ViL’s guidance, followed by constructing a Denoised-Region that leverages the relative independence between the ViL and the adapting model to decrease noise. Experiments on Office-Home, VisDA, and DomainNet-126 show that TS-DRD achieves competitive or better performance than existing source-dependent SFDA methods. By eliminating all dependencies on the source domain, VODA offers a more practical and resource-efficient solution for the adaptation of the real-world domain.

6. Acknowledgements

This work was supported by the 2024 Hubei Provincial Department of Education Scientific Research Program for Young Talents under (Q20241903), the Outstanding Youth Science and Technology Innovation Team Project for Colleges and Universities of Hubei Province of China (T2023013), Natural Science Foundation of Hubei Province of China (2023AFD061) and the Enshi Prefecture’s 2023 Technology Support Category Science and Technology Plan Projects (D20230065).

References

- [1] J. Liang, D. Hu, J. Feng, Do we really need to access the source data? source hypothesis transfer for unsupervised domain adaptation, in: Proceedings of the 37th International Conference on Machine Learning, ICML’20, JMLR.org, 2020, pp. 6028–6039. doi:10.48550/arXiv.2002.08546.
URL <https://doi.org/10.48550/arXiv.2002.08546>
- [2] J. Li, Z. Yu, Z. Du, L. Zhu, H. T. Shen, A comprehensive survey on source-free domain adaptation, IEEE Transactions on Pattern Analysis and Machine Intelli-

- gence 46 (8) (2024) 5743–5762. doi:10.1109/TPAMI.2024.3370978.
URL <https://doi.org/10.1109/TPAMI.2024.3370978>
- [3] J. Li, Y. Li, Y. Fu, J. Liu, Y. Liu, M. Yang, I. King, Clip-powered domain generalization and domain adaptation: A comprehensive survey, *IEEE Transactions on Pattern Analysis and Machine Intelligence* (2026) 1–20doi:10.1109/TPAMI.2026.3651700.
URL <https://doi.org/10.1109/TPAMI.2026.3651700>
- [4] S. Tang, W. Su, M. Ye, X. Zhu, Source-free domain adaptation with frozen multimodal foundation model, in: *Proceedings of the IEEE/CVF Conference on Computer Vision and Pattern Recognition, CVPR '24*, 2024, pp. 23711–23720. doi:10.48550/arXiv.2311.16510.
URL <https://doi.org/10.48550/arXiv.2311.16510>
- [5] S. Tang, W. Su, Y. Gan, M. Ye, J. Dr. Zhang, X. Zhu, Proxy denoising for source-free domain adaptation, in: *International Conference on Representation Learning*, 2025, pp. 82548–82569. doi:10.48550/arXiv.2406.01658.
URL <https://doi.org/10.48550/arXiv.2406.01658>
- [6] M. Zhan, Z. Wu, J. Yang, L. Peng, J. Shen, X. Zhu, Dual transferable knowledge interaction for source-free domain adaptation, *Information Processing & Management* 63 (1) (2026) 104302. doi:10.1016/j.ipm.2025.104302.
URL <https://doi.org/10.1016/j.ipm.2025.104302>
- [7] S. Yang, J. Van de Weijer, L. Herranz, S. Jui, et al., Exploiting the intrinsic neighborhood structure for source-free domain adaptation, in: *Advances in Neural Information Processing Systems*, Vol. 34 of *NeurIPS '21*, 2021, pp. 29393–29405. doi:10.48550/arXiv.2110.04202.
URL <https://doi.org/10.48550/arXiv.2110.04202>
- [8] F. You, J. Li, L. Zhu, Z. Chen, Z. Huang, Domain adaptive semantic segmentation without source data, in: *Proceedings of the 29th ACM International Conference on Multimedia, MM '21*, ACM, 2021, pp. 3293–3302. doi:10.1145/3474085.

3475482.

URL <https://doi.org/10.1145/3474085.3475482>

- [9] I. Diamant, A. Rosenfeld, I. Achituve, J. Goldberger, A. Netzer, De-confusing pseudo-labels in source-free domain adaptation, in: European Conference on Computer Vision, Springer, 2024, pp. 108–125. doi:10.48550/arXiv.2401.01650.
URL <https://doi.org/10.48550/arXiv.2401.01650>
- [10] V. K. Kurmi, V. K. Subramanian, V. P. Namboodiri, Domain impression: A source data free domain adaptation method, in: Proceedings of the IEEE/CVF Winter Conference on Applications of Computer Vision, WACV '21, IEEE, 2021, pp. 615–625. doi:10.1109/WACV48630.2021.00066.
URL <https://doi.org/10.1109/WACV48630.2021.00066>
- [11] J. Huang, D. Guan, A. Xiao, S. Lu, Model adaptation: Historical contrastive learning for unsupervised domain adaptation without source data, in: Advances in Neural Information Processing Systems, Vol. 34 of NeurIPS '21, 2021, pp. 3635–3649. doi:10.48550/arXiv.2110.03374.
URL <https://doi.org/10.48550/arXiv.2110.03374>
- [12] N. Ding, Y. Xu, Y. Tang, C. Xu, Y. Wang, D. Tao, Source-free domain adaptation via distribution estimation, in: Proceedings of the IEEE/CVF Conference on Computer Vision and Pattern Recognition, CVPR '22, IEEE, New Orleans, LA, USA, 2022, pp. 7202–7212. doi:10.1109/CVPR52688.2022.00707.
URL <https://doi.org/10.1109/CVPR52688.2022.00707>
- [13] Y. Du, H. Yang, M. Chen, H. Luo, J. Jiang, Y. Xin, C. Wang, Generation, augmentation, and alignment: A pseudo-source domain based method for source-free domain adaptation, Machine Learning 113 (6) (2024) 3611–3631. doi:10.1007/s10994-023-06432-8.
URL <https://doi.org/10.1007/s10994-023-06432-8>
- [14] A. Radford, J. W. Kim, C. Hallacy, A. Ramesh, G. Goh, S. Agarwal, G. Sastry, A. Askell, P. Mishkin, J. Clark, et al., Learning transferable visual models from

- natural language supervision, in: International conference on machine learning, PmLR, 2021, pp. 8748–8763. doi:10.48550/arXiv.2103.00020.
URL <https://doi.org/10.48550/arXiv.2103.00020>
- [15] C. Ge, R. Huang, M. Xie, Z. Lai, S. Song, S. Li, G. Huang, Domain adaptation via prompt learning, *IEEE Transactions on Neural Networks and Learning Systems* 36 (1) (2025) 1160–1170. doi:10.1109/TNNLS.2023.3327962.
URL <https://doi.org/10.1109/TNNLS.2023.3327962>
- [16] K. Zhou, J. Yang, C. C. Loy, Z. Liu, Learning to prompt for vision-language models, *International Journal of Computer Vision* 130 (9) (2022) 2337–2348. doi:10.1007/s11263-022-01653-1.
URL <https://doi.org/10.1007/s11263-022-01653-1>
- [17] M. Shu, W. Nie, D.-A. Huang, Z. Yu, T. Goldstein, A. Anandkumar, C. Xiao, Test-time prompt tuning for zero-shot generalization in vision-language models, in: *Advances in Neural Information Processing Systems*, 2022, pp. 14274–14289. doi:10.48550/arXiv.2209.07511.
URL <https://doi.org/10.48550/arXiv.2209.07511>
- [18] T. Meng, X. Jing, Z. Yan, W. Pedrycz, A survey on machine learning for data fusion, *Information Fusion* 57 (2020) 115–129. doi:10.1016/j.inffus.2019.12.001.
URL <https://doi.org/10.1016/j.inffus.2019.12.001>
- [19] H. M. Gomes, J. P. Barddal, F. Enembreck, A. Bifet, A survey on ensemble learning for data stream classification, *ACM Computing Surveys* 50 (2) (2017). doi:10.1145/3054925.
URL <https://doi.org/10.1145/3054925>
- [20] X. Ji, J. F. Henriques, A. Vedaldi, Invariant information clustering for unsupervised image classification and segmentation, in: *Proceedings of the IEEE/CVF international conference on computer vision*, 2019, pp. 9865–9874. doi:10.48550/arXiv.1807.06653.
URL <https://doi.org/10.48550/arXiv.1807.06653>

- [21] W. Hu, T. Miyato, S. Tokui, E. Matsumoto, M. Sugiyama, Learning discrete representations via information maximizing self-augmented training, in: Proceedings of the 34th International Conference on Machine Learning, ICML'17, JMLR.org, Sydney, Australia, 2017, pp. 1558–1567. doi:10.48550/arXiv.1702.08720.
URL <https://doi.org/10.48550/arXiv.1702.08720>
- [22] H. Venkateswara, J. Eusebio, S. Chakraborty, S. Panchanathan, Deep hashing network for unsupervised domain adaptation, in: Proceedings of the IEEE Conference on Computer Vision and Pattern Recognition, CVPR '17, IEEE, Honolulu, HI, USA, 2017, pp. 5385–5394. doi:10.1109/CVPR.2017.572.
URL <https://doi.org/10.1109/CVPR.2017.572>
- [23] X. Peng, B. Usman, N. Kaushik, J. Hoffman, D. Wang, K. Saenko, Visda: The visual domain adaptation challenge, arXiv preprint arXiv:1710.06924 (2017). doi:10.48550/arXiv.1710.06924.
URL <https://doi.org/10.48550/arXiv.1710.06924>
- [24] T.-Y. Lin, M. Maire, S. Belongie, J. Hays, P. Perona, D. Ramanan, P. Dollár, C. L. Zitnick, Microsoft coco: Common objects in context, in: European conference on computer vision, Springer, 2014, pp. 740–755. doi:10.48550/arXiv.1405.0312.
URL <https://doi.org/10.48550/arXiv.1405.0312>
- [25] X. Peng, Q. Bai, X. Xia, Z. Huang, K. Saenko, B. Wang, Moment matching for multi-source domain adaptation, in: Proceedings of the IEEE/CVF International Conference on Computer Vision, ICCV '19, IEEE, Seoul, South Korea, 2019, pp. 1406–1415. doi:10.1109/ICCV.2019.00149.
URL <https://doi.org/10.1109/ICCV.2019.00149>
- [26] S. Tang, Y. Shi, Z. Ma, J. Li, J. Lyu, Q. Li, J. Zhang, Model adaptation through hypothesis transfer with gradual knowledge distillation, in: 2021 IEEE/RSJ International Conference on Intelligent Robots and Systems (IROS), IEEE, 2021, pp.

5679–5685. doi:10.1109/IR0S51168.2021.9636206.

URL <https://doi.org/10.1109/IR0S51168.2021.9636206>

- [27] S. Yang, S. Jui, J. Van De Weijer, et al., Attracting and dispersing: A simple approach for source-free domain adaptation, in: *Advances in Neural Information Processing Systems*, Vol. 35 of *NeurIPS '22*, New Orleans, Louisiana, USA, 2022, pp. 6000–6010. doi:10.48550/arXiv.2205.04183.
URL <https://doi.org/10.48550/arXiv.2205.04183>
- [28] D. Chen, D. Wang, T. Darrell, S. Ebrahimi, Contrastive test-time adaptation, in: *Proceedings of the IEEE/CVF Conference on Computer Vision and Pattern Recognition*, 2022, pp. 295–305. doi:10.48550/arXiv.2204.10377.
URL <https://doi.org/10.48550/arXiv.2204.10377>
- [29] J. Lee, D. Jung, J. Yim, S. Yoon, Confidence score for source-free unsupervised domain adaptation, in: *International conference on machine learning*, PMLR, 2022, pp. 12365–12377. doi:10.48550/arXiv.2206.06640.
URL <https://doi.org/10.48550/arXiv.2206.06640>
- [30] L. Yi, G. Xu, P. Xu, J. Li, R. Pu, C. Ling, A. I. McLeod, B. Wang, When source-free domain adaptation meets learning with noisy labels, in: *International Conference on Representation Learning*, 2023. doi:10.48550/arXiv.2301.13381.
URL <https://doi.org/10.48550/arXiv.2301.13381>
- [31] M. Litrico, A. Del Bue, P. Morerio, Guiding pseudo-labels with uncertainty estimation for source-free unsupervised domain adaptation, in: *Proceedings of the IEEE/CVF Conference on Computer Vision and Pattern Recognition*, 2023, pp. 7640–7650. doi:10.48550/arXiv.2303.03770.
URL <https://doi.org/10.48550/arXiv.2303.03770>
- [32] L. Zhou, N. Li, M. Ye, X. Zhu, S. Tang, Source-free domain adaptation with class prototype discovery, *Pattern Recognition* 145 (2024) 109974. doi:10.1016/j.patcog.2023.109974.
URL <https://doi.org/10.1016/j.patcog.2023.109974>

- [33] S. Tang, A. Chang, F. Zhang, X. Zhu, M. Ye, C. Zhang, Source-free domain adaptation via target prediction distribution searching, *International Journal of Computer Vision* 132 (3) (2024) 654–672. doi:10.1007/s11263-023-01892-w. URL <https://doi.org/10.1007/s11263-023-01892-w>
- [34] G. Xu, H. Guo, L. Yi, C. Ling, B. Wang, G. Yi, Revisiting source-free domain adaptation: a new perspective via uncertainty control, in: *The Thirteenth International Conference on Learning Representations, 2025*. URL https://proceedings.iclr.cc/paper_files/paper/2025/file/e85454a113e8b41e017c81875ae68d47-Paper-Conference.pdf
- [35] R. Shao, W. Zhang, K. Luo, Q. Li, J. Wang, Consistent assistant domains transformer for source-free domain adaptation, *IEEE Transactions on Image Processing* (2025). doi:10.1109/TIP.2025.3611799. URL <https://doi.org/10.1109/TIP.2025.3611799>
- [36] Z. Lai, N. Vedapunt, N. Zhou, J. Wu, C. P. Huynh, X. Li, K. K. Fu, C.-N. Chuah, Padclip: Pseudo-labeling with adaptive debiasing in clip for unsupervised domain adaptation, in: *Proceedings of the IEEE/CVF International Conference on Computer Vision, 2023*, pp. 16155–16165. doi:10.1109/ICCV51070.2023.01480. URL <https://doi.org/10.1109/ICCV51070.2023.01480>
- [37] M. Singha, H. Pal, A. Jha, B. Banerjee, Ad-clip: Adapting domains in prompt space using clip, in: *Proceedings of the IEEE/CVF International Conference on Computer Vision, 2023*, pp. 4355–4364. doi:10.48550/arXiv.2308.05659. URL <https://doi.org/10.48550/arXiv.2308.05659>
- [38] Z. Du, X. Li, F. Li, K. Lu, L. Zhu, J. Li, Domain-agnostic mutual prompting for unsupervised domain adaptation, in: *Proceedings of the IEEE/CVF Conference on Computer Vision and Pattern Recognition, 2024*, pp. 23375–23384. doi:10.48550/arXiv.2403.02899. URL <https://doi.org/10.48550/arXiv.2403.02899>
- [39] S. Bai, M. Zhang, W. Zhou, S. Huang, Z. Luan, D. Wang, B. Chen, Prompt-based distribution alignment for unsupervised domain adaptation, in: *Proceedings*

- of the AAAI conference on artificial intelligence, Vol. 38, 2024, pp. 729–737.
doi:10.48550/arXiv.2312.09553.
URL <https://doi.org/10.48550/arXiv.2312.09553>
- [40] P. P. Busto, J. Gall, Open set domain adaptation, in: 2017 IEEE INTERNATIONAL CONFERENCE ON COMPUTER VISION, 2017, pp. 754–763. doi:10.1109/ICCV.2017.88.
URL <https://doi.org/10.1109/ICCV.2017.88>
- [41] K. He, X. Zhang, S. Ren, J. Sun, Deep residual learning for image recognition, in: Proceedings of the IEEE Conference on Computer Vision and Pattern Recognition, CVPR '16, IEEE, Las Vegas, NV, USA, 2016, pp. 770–778. doi:10.1109/CVPR.2016.90.
URL <https://doi.org/10.1109/CVPR.2016.90>
- [42] X. Glorot, Y. Bengio, Understanding the difficulty of training deep feedforward neural networks, *Journal of Machine Learning Research* 9 (2010) 249–256.
- [43] S. Ioffe, C. Szegedy, Batch normalization: Accelerating deep network training by reducing internal covariate shift, in: 32nd International Conference on Machine Learning, 2015, pp. 448–456. doi:10.48550/arXiv.1502.03167.
URL <https://doi.org/10.48550/arXiv.1502.03167>
- [44] A. Dosovitskiy, An image is worth 16x16 words: Transformers for image recognition at scale, arXiv preprint arXiv:2010.11929 (2020). doi:10.48550/arXiv:2010.11929.
URL <https://doi.org/10.48550/arXiv:2010.11929>
- [45] A. Vaswani, N. Shazeer, N. Parmar, J. Uszkoreit, L. Jones, A. N. Gomez, Ł. Kaiser, I. Polosukhin, Attention is all you need, in: Advances in Neural Information Processing Systems, Vol. 31 of NeurIPS '17, Long Beach, California, USA, 2017, pp. 6000–6010. doi:10.48550/arXiv.1706.03762.
URL <https://doi.org/10.48550/arXiv.1706.03762>